State of Delaware
DELAWARE GEOLOGICAL SURVEY
David R. Wunsch, State Geologist

BULLETIN NO. 21D

USING NUMERICAL MODELS TO ASSESS A RAPID INFILTRATION BASIN SYSTEM (RIBS), CAPE HENLOPEN STATE PARK, DELAWARE

By

Changming He,
Scott Andres

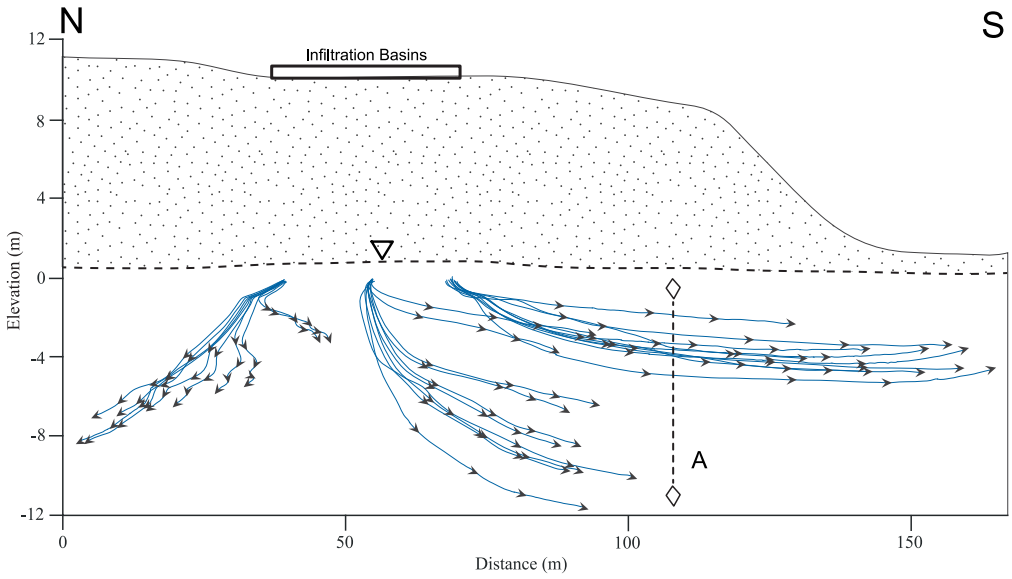

Delaware Geological Survey
University of Delaware
Newark, Delaware
2015

TABLE OF CONTENTS

Page

ABSTRACT 1

INTRODUCTION 1

Purpose and Scope 1

Acknowledgments 2

SITE DESCRIPTION AND METHODS 2

Field Methods 2

Groundwater Model Development 4

Boundary conditions 4

Hydraulic properties 4

Precipitation and recharge 4

Wastewater discharge 4

Contaminant transport simulation 4

RESULTS AND DISCUSSION 7

Calibration Results 7

Mounding Analysis 9

Mass Balance Analysis of N and P 10

Sensitivity Analysis 10

Comparison of 2-D and 3-D Particle Pathlines 10

CONCLUSIONS 12

REFERENCES CITED 13

ILLUSTRATIONS

Page

Figure 1. Location of study area....2
Figure 2. Conceptual hydrogeologic model showing Holocene sediments beneath the RIBS at Cape Henlopen State Park 3....3
Figure 3. Model domain and location of RIBS shown on a 2007 aerial photograph of Cape Henlopen, Delaware....3
Figure 4. Monthly discharge rates to the infiltration basins....4
Figure 5. Conceptualized nitrogen pathways in the unsaturated zone before discharged effluent reaches the water table. 5
Figure 6. Total nitrogen and phosphorous concentrations of effluent in grab samples taken directly from discharge pipes in the RIBS....6
Figure 7. Degree of phosphorous saturation calculated using M3-PSR method....6
Figure 8. Comparison of observed and simulated water-table elevations for monitoring wells Ni45-35, Ni45-36, Ni45-37 and Ni45-45....8
Figure 9. Comparison of observed and simulated NO_3^--N and OP for monitoring wells Ni45-36 and Ni45-37....8
Figure 10. Comparison of observed and simulated NO_3^--N and OP concentrations at well Ni45-35 and CMT3....8
Figure 11. Comparison of observed and simulated NO_3^--N and OP concentrations at well Ni45-45 and CMT2....9
Figure 12. Comparison of maximum groundwater mounding beneath RIBS computed by analytical and numerical modeling methods....10
Figure 13. Plot of sensitivity analysis results for the calibrated model testing hydraulic conductivity, decay rate (for NO_3^--N)/sorption coefficient (for OP), recharge concentrations of wastewater, dispersion, and wastewater recharge rate....10
Figure 14. Particle pathlines computed by the 2-D steady-state model....11
Figure 15. Particle pathlines computed by the 3-D model....11
Figure 16. Cross-sectional view of particle pathlines computed by the 3-D model....12

TABLES

Table 1. Precipitation recorded between June 2008 and June 2009 at the REC station in Georgetown, Delaware....4
Table 2. Discharge rates in the RIBS during the simulation period....5
Table 3. Calibrated parameter values....7
Table 4. Parameters used in Hantush analytical method to calculate mounding height....9

Use of trade, product, or firm names in this report is for descriptive purposes only and does not imply endorsement by the Delaware Geological Survey.

USING NUMERICAL MODELS TO ASSESS A RAPID INFILTRATION BASIN SYSTEM (RIBS), CAPE HENLOPEN STATE PARK, DELAWARE

ABSTRACT

The long-term performance of rapid infiltration basin systems (RIBS) and their potential impacts on the receiving environment have been previously unknown for Delaware. A variety of field experiments were conducted to characterize the geology and hydrogeology of a RIBS facility that has been in operation for more than 20 years at Cape Henlopen State Park. Pairs of standard monitoring wells and short-screened multi-level wells were used to evaluate the significance of small-scale vertical variability in water quality. A three-dimensional transient groundwater flow and contaminant transport model was constructed to simulate the groundwater mounding and the movements of nitrate-nitrogen (NO_3^--N) and orthophosphorus (OP) in the groundwater. In the numerical model, NO_3^--N was treated as a reactive species and denitrification was simulated with a first-order degradation rate constant. The major mechanism affecting OP transport in groundwater is sorption/desorption, which was simulated using a linear sorption isotherm. Simulated concentrations reasonably fit observed concentrations of NO_3^--N and OP in both standard wells and multi-level wells. The calibrated model predicts that with a denitrification rate of 0.006/day and a distribution coefficient of 4×10^{-7} L/mg, 63 percent of the reduction in the mass of NO_3^--N is attributable to denitrification, and more than 99 percent of OP is detained in the aquifer due to sorption on subsurface solids. However, the long-term operation of RIBS has led to a reduction of the sorption capacity of subsurface solids for phosphorous, resulting in significant concentrations of OP in groundwater adjacent to RIBS.

INTRODUCTION

Rapid infiltration basin systems (RIBS) consist of several simple and fairly standard technologies employed for the land-based disposal of wastewater (Crites et al., 2006). In most cases, domestic wastewater generated by parks, homes, and businesses is collected and conveyed to a treatment plant. Following chemical and physical treatment of the wastewater, the effluent is discharged to an unlined infiltration basin. When design criteria are met, the effluent quickly infiltrates into the soil, where the vadose zone acts to filter suspended solids, biodegradable materials, bacteria, viruses, and other microorganisms (Crites et al., 2006; Asano et al., 2007). Nitrogen (N), phosphorus (P), organic compounds, and heavy metal concentrations may be significantly reduced if the infiltration rates and biogeochemical properties of the effluent are well matched to the capacity of the vadose zone to attenuate these contaminants. Subject to the same controls that constrain contaminant attenuation in the vadose zone, additional physical, chemical, and biological treatment can occur in the underlying aquifer. Asano et al. (2007) use the term soil-aquifer treatment (SAT) for this system. In many locations around the world, water from SAT systems is reclaimed for agriculture, horticulture, maintaining surface-water flow, sustaining important subaqueous and wetland habitat, and industrial uses (Crites et al., 2006).

The risk of groundwater contamination is greater when inadequately treated effluent infiltrates and flows without effective SAT. This is of concern in Delaware, where the receiving water body, the Columbia aquifer, is the source of drinking water and provides 60 to 80 percent of the streamflow over a large area (Johnston, 1976; Guitierrez-Magness and Raffensperger, 2003). Nearly 40 years of research by academic, state, and federal scientists has documented that the Columbia aquifer is highly susceptible to contamination from the application of wastes onto and into the ground. The contaminants persist in the groundwater for decades, where they commonly impact potable water supply wells (Miller, 1972; Robertson, 1977; Ritter and Chirnside, 1984; Andres, 1991; Pellerito et al., 2006), eventually discharge into bodies of surface water, leading to well-documented eutrophication problems (Guitierrez-Magness and Raffensperger, 2003; Denver et al., 2004). Debrewer et al. (2005) and Ator (2008) found that Delaware's water-quality problems and their causes are consistent with those observed throughout Delmarva and much of the Mid-Atlantic Coastal Plain.

Purpose and Scope

In many states, groundwater monitoring systems are required for permit compliance at RIBS facilities. These systems range in sophistication from three or four single-screen wells to larger arrays of wells finished at multiple depths. In this study, pairs of standard monitoring wells and short-screened multi-level wells were used to evaluate the significance of small-scale vertical variability in water quality.

In Delaware, groundwater-flow models are frequently used in the development of facility designs, especially to determine if the proposed designs can meet state-required separation distances between the bottom of the infiltration beds and the mounded water table. Other states require models, with the level of sophistication determined on a case-by-case basis. Coupled flow and contaminant transport models are less frequently used, even though they are well suited for exploring and evaluating the risks associated with RIBS, assisting with the design of compliance monitoring systems, and post-auditing the conceptual hydrogeologic models and geochemical assumptions used in the development of facility designs.

In this study, a RIBS site located on a shallow, unconfined aquifer was monitored to evaluate the risks of RIBS on the environment. Monitoring results were used to construct,

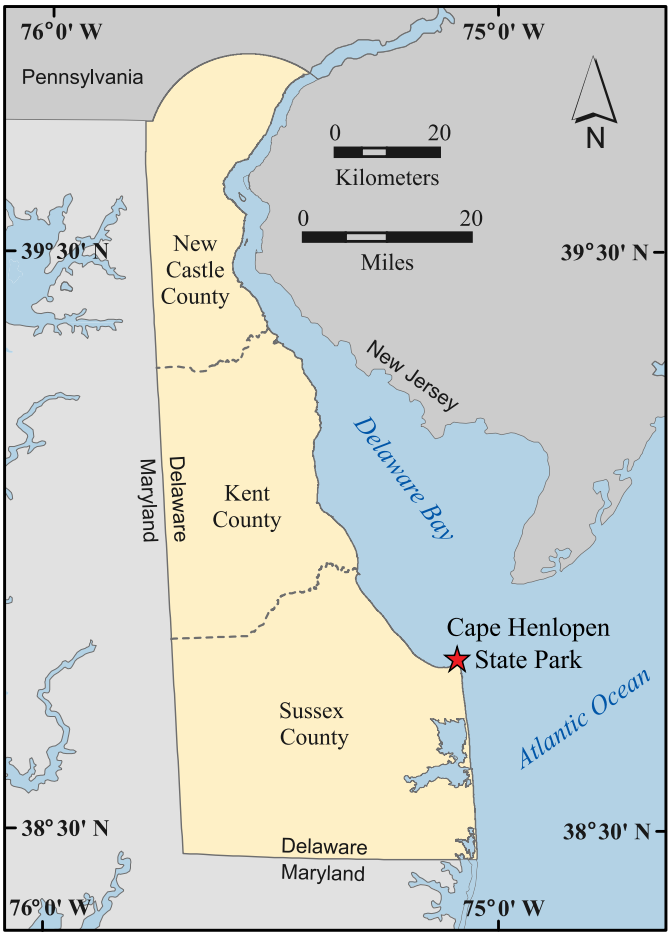

Figure 1. Location of study area.

calibrate, and test a three-dimensional (3-D) numerical flow and transport simulation. Flow simulation results were compared to the results from analytic models of groundwater mounding. Results of the simplified transport simulations were used to assess how well these simplifications can reproduce monitoring results and approximate the more complex major mechanisms of nitrate-nitrogen (NO_3^--N) and orthophosphorus (OP) attenuation or persistence in groundwater.

Acknowledgments

This work was funded by the Delaware Department of Natural Resources and Environmental Control (DNREC) and the Delaware Geological Survey (DGS). John H.Talley and the DNREC Groundwater Protection Branch, coordinated by Scott Strohmeier, reviewed this document and provided helpful comments. Lillian T. Wang provided technical assistance on the figures in this document.

SITE DESCRIPTION AND METHODS

The selected RIBS facility is located at Cape Henlopen State Park (CHSP), Sussex County, Delaware (Fig. 1). The CHSP RIBS is sited on unnamed Holocene dune deposits that are predominately composed of quartz sand with trace amounts of quartzose granules. The thickness of the dune deposits range from a featheredge at the toe of the dune to about 13.7 m at the top of the dune (Fig. 2). Directly beneath the dune deposits are interbedded swamp/marsh deposits, which range from silty, peaty sands to sandy, silty peats with scattered logs; partially carbonized wood fragments, charcoal, and pebbles (Andres et al., 2015); and spit deposits consisting of coarse- to medium-sand with variable amounts of fine- to-medium gravel and medium-to-coarse sand. Unnamed Holocene marine deposits consisting of interbedded sandy muds, muds, and silty fine sands underlie the spit deposits and form the base of the aquifer. The water table is located 8 to 9 m beneath the RIBS. In the conceptual model for the site (Fig. 2) the dune, swamp/marsh, and spit deposits function as an unconfined aquifer and Holocene marine deposits function as a confining bed that forms the base of the unconfined aquifer.

The wastewater system serves a beach bathhouse, visitor center, and dormitories. Pretreatment consists of two Imhoff tanks operated in sequence, with the first tank functioning aerobically, and the second anaerobically, and chlorination prior to discharge (Lee McDaniel, personal comm.). Effluent is discharged to eight infiltration basins (Fig. 3), each with six discharge points. Because there is very little storage in the system, discharge occurs in frequent doses, with the frequency dependent on influent flow rates. A mechanical valve system controls which infiltration bed receives effluent and switches between beds roughly every day (Lee McDaniel, personal comm.), giving each bed one day of flooding followed by a seven-day resting period. The resting period allows any organic material that collects on the soil surface to dry and begin to decay, allows the soil to dry and reaerate, and also promotes the mineralization of organic N and P, and the nitrification of ammonia nitrogen (U.S. Environmental Protection Agency, 2006). The infiltration basins have been used since 1983 and the operational schedule has not been significantly modified since the facility's inception.

Field Methods

Beginning in February 2007, test borings and monitoring wells were installed at nine locations in the study site (Fig. 3). Seven-channel multi-level wells (CMT System - Solinst Canada) were installed at four locations next to the standard wells. Standard wells were constructed with 5.1-cm diameter schedule 40 PVC pipe and 4.6-m long slotted well screen. Each of the CMT sample ports is 0.1 m long and set from near the top of the well screen to just below the bottom of the well screen. In-Situ Troll-300© data loggers were placed in standard monitoring wells to monitor groundwater level and temperature. Eight sets of water samples were collected from wells and surface water between April 2008 and November 2009. Sampling methods were adapted from those used in previous groundwater (Sims et al., 1996) and surface water studies (Ullman et al., 2002). During this project, field measurements of pH, temperature (T), specific conductance (SC), and dissolved oxygen (DO) were made with an YSI 556 MPS. Groundwater samples were filtered in the field through 0.4-micron polyester-fiber capsules (Geotech). The University of Delaware Bioresources Engineering Department Water Quality Laboratory performed analyses of NO_3^--N, ammonium-nitrogen, Kjeldahl-nitrogen, and OP. The field-measured groundwater heads and sampling results were used

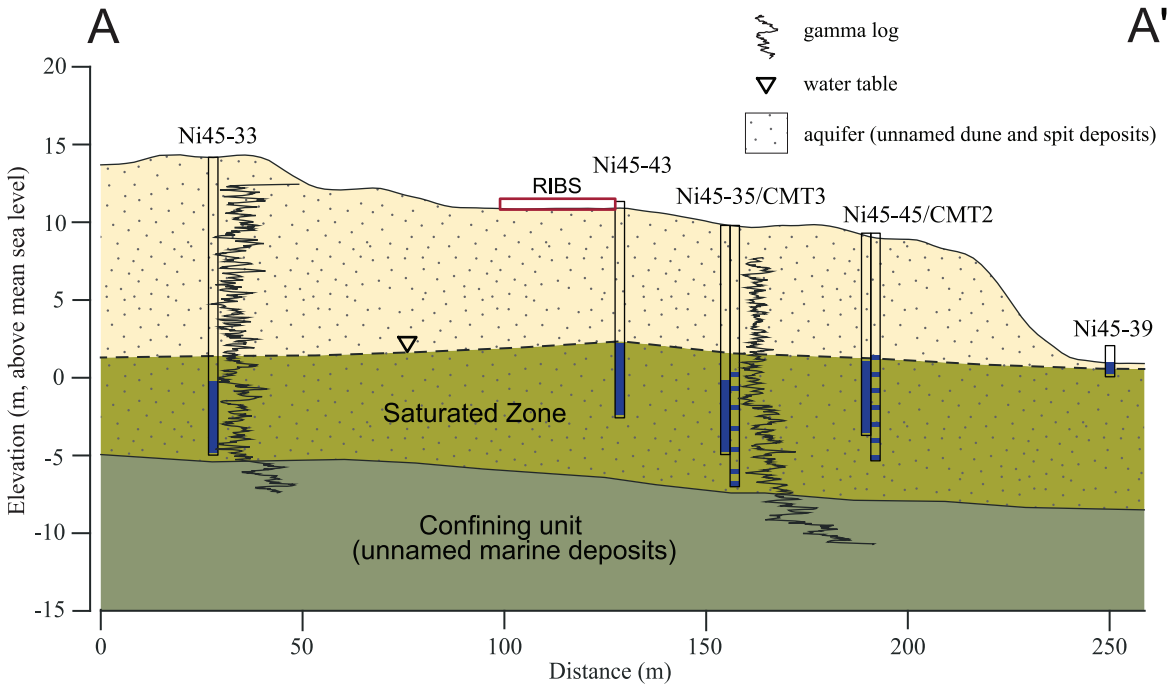

Figure 2. Conceptual hydrogeologic model showing Holocene sediments beneath the RIBS at Cape Henlopen State Park. Line of cross section is shown in Figure 3. Cross-section line, wells, and CMTs were used for model calibration. Screens of standard wells are shown in solid blue. Screens of CMT sample ports are shown as dark, horizontal lines.

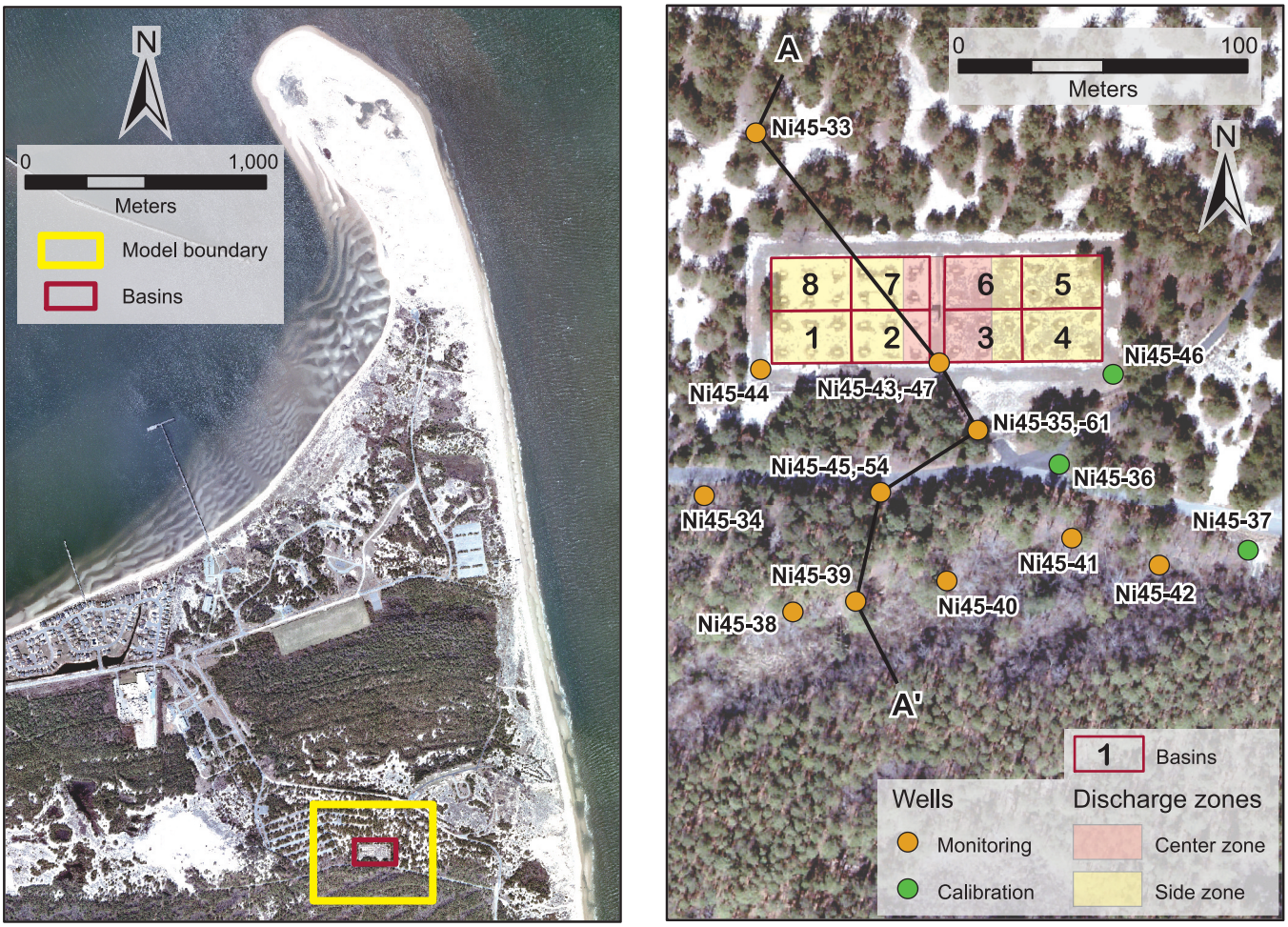

Figure 3. Model domain and location of RIBS shown on a 2007 aerial photograph of Cape Henlopen, Delaware. Coordinates (UTM18-83 in m) of the model domain are easting minimum 491,600, easting maximum 492,100, northing minimum 4,291,600, northing maximum 4,292,000. The figure on the right shows locations of monitoring and calibration wells, basins, discharge zones, and line of cross section shown on the aerial photograph.

Table 1. Precipitation recorded between June 2008 and June 2009 at the weather station in Georgetown, Delaware (National Weather Service ID: KGED).

Time Period	Total precipitation (cm)
Jun – Oct	33
Nov – Jan	29
Feb – Apr	13
May – Jun	28

to set up the initial conditions for the groundwater flow and contaminant transport models and to calibrate the models.

Groundwater Model Development

A 3-D transient groundwater model was developed to simulate the groundwater flow and N and P transport from the RIBS for a one-year period from June 2008 to May 2009. The model was constructed using MODFLOW 2000 and MT3DMS in combination with Visual Modflow 2009.1 as the pre-and post-processors. The model domain covers an area of 200,000 m^2 with the RIBS located in the center (Fig. 3). The domain is discretized into a three-layer grid consisting of 100 rows and 125 columns, with each cell having dimensions of 4 m by 4 m.

Dune deposits are assigned to the top layer of the model. Interbedded swamp/marsh and spit deposits are assigned to the second and third layers. Unnamed Holocene marine deposits act as the lower no-flow boundary for the model.

Boundary conditions

Because there are no natural physical boundaries adjacent to the RIBS, general head boundaries (GHB) were assigned to the east, north, and west sides of the model domain. To the south, where there is a swamp, a specified head boundary was assigned. The swamp discharges water towards the west into a tidal water body when heads in the swamp exceed about 0.3 m. Head values for the swamp were obtained from field measurements in monitoring wells between 2008 and 2009.

Hydraulic properties

Grain size tests show that the dune deposit sands are relatively uniform, with a mean grain size of 1.2 mm (range 0.68 - 1.62 mm) and a standard deviation of 0.57 mm. Slug tests were conducted in 15 different monitoring wells, and the results were analyzed by the method described by Bouwer (1989). Hydraulic conductivity (K) values range from 6 m/day to 55 m/day with a median value 31 m/day. K values of dune deposits tended to be higher (> 30 m/day) than those of the spit and marsh/swamp deposits (< 15 m/day). These values were assigned to the model and adjusted during calibration.

Precipitation and recharge

Precipitation data measured at Georgetown, Delaware, (National Weather Service ID: KGED) were used to assign initial recharge rates. In the model, recharge was aggregated into four time periods (Table 1). Recharge rates were adjusted during calibration.

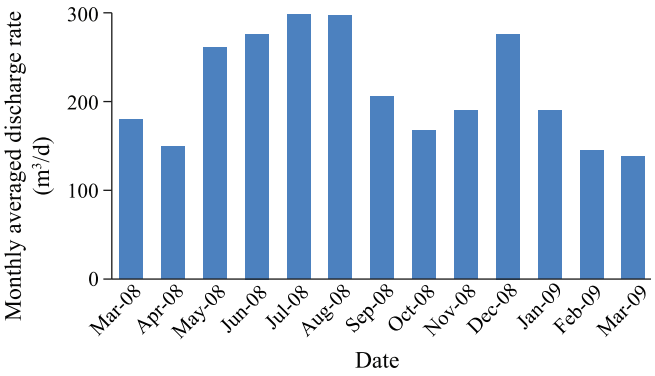

Figure 4. Monthly discharge rates to the infiltration basins. Data were provided by the wastewater plant operator.

Wastewater discharge

The monthly rates of wastewater discharged to the infiltration basins during the period March 2008 to March 2009 show seasonal variations (Fig. 4). From the end of April to the end of August, when the number of park visitors was greatest, the average discharge rate was 280 m^3/d; whereas during October through March, the average discharge rate was approximately 170 m^3/d. The infiltration of groundwater into the wastewater collection system is a problem during periods when the water table is high (Lee McDaniel, personal comm.). During the study period, the total volume of discharge was 82,598 m^3. To simplify the simulation, the eight sub-basins were divided into two zones according to the discharge schedule: one center zone with a larger discharge rate and two side zones with smaller discharge rates (Fig. 3). The initial annual discharge rates applied on each zone are shown in Table 2.

The calibrated model predicts that 10 to 40 percent of precipitation and 70 to 80 percent of discharged wastewater enters the groundwater system through the recharge boundary. The natural precipitation rates are consistent with those determined by hydrograph separation and water-budget techniques (Johnston, 1976). The difference between simulated and observed effluent discharge rates is thought to be due in part to evaporation; however, errors in the measurement of effluent volume cannot be discounted.

Contaminant transport simulation

The movement and transformation of the two major dissolved contaminants detected in groundwater (NO_3^--N and OP) were simulated using MT3DMS. Because MT3DMS is a package designed to simulate contaminant transport in the saturated zone, the movements and transformations of contaminants in the unsaturated zone will not be simulated. The N-cycle in the unsaturated zone beneath the RIBS is very complex (Fig. 5) since many factors affect nitrate leaching into the water table (Ling and Ei-Kadi, 1998, Heatwole and McCray, 2007). P exists in different forms in the vadose zone as well. The magnitude and direction of transformations between each component are controlled by complex biogeochemical processes, complicated in part by the heterogeneity of the porous media. Field data indicate

Table 2. Wastewater discharge rates on the infiltration basins during the simulation period. The initial values were calculated based on wastewater plant records. The total area of the infiltration beds is 3,584 m^2.

Time Period	Discharge Rate (cm/year)			
	Center Zone		Side Zones	
	Initial	Calibrated	Initial	Calibrated
Jun. – Aug.	5182	3701	2073	1481
Sep. – Nov.	3630	2652	1453	1062
Dec.	5964	4656	2385	1862
Jan. – Mar.	2824	2248	1133	899
Apr. – Jun.	4884	3807	1953	1524

that a vast majority of the total N and total P in effluent have been converted to NO_3^--N and OP prior to reaching the water table (Andres et al., 2015). As a result, we used the total N and total P in effluent samples as the recharge concentration of NO_3^--N and OP (Fig. 6). Initial concentrations of NO_3^--N and OP in the aquifer were determined by gridding results of June 2008 sample data using Surfer (Golden Software, 2008) with the ordinary kriging algorithm.

The governing equation describes the fate and transport of aqueous- and solid-phase species in multi-dimensional saturated porous media (Zheng and Wang, 1999):

$$\frac{\partial(\theta C)}{\partial t} = \frac{\partial}{\partial x_i}\left(\theta D_{ij}\frac{\partial C}{\partial x_j}\right) - \frac{\partial}{\partial x_i}(\theta v_i C) + q_s C_s + \sum R_n \quad (1)$$

Where:

C Dissolved concentration of species (N, P, et al.), ML^{-3};

θ Porosity, dimensionless;

t Time, T;

x_i Distance along the respective Cartesian coordinate axis, L;

D_{ij} Hydrodynamic dispersion coefficient tensor, L^2 T^{-1};

v_i Seepage or linear pore water velocity, LT^{-1};

q_i Volumetric flow rate per unit volume of aquifer representing fluid sources (positive) and sinks (negative), T^{-1};

C_s Concentration of the source or sink flux for species, MT^{-3};

$\sum R_n$ Chemical reactions, ML^{-3} T^{-1}. Different species have different reaction forms due to the biochemical properties of the species and to the aquifers.

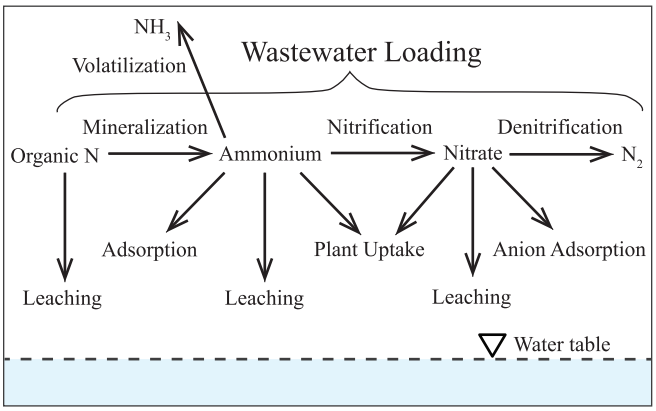

Figure 5. Conceptualized nitrogen pathways in the unsaturated zone before discharged effluent reaches the water table.

Many studies of NO_3^--N transformations in groundwater have concluded that the anion is quite soluble in water and is not significantly adsorbed by clay-rich soils; NO_3^--N may be reduced to nitrogen gas by multiple denitrification processes that occur primarily in anoxic conditions and involve heterotrophic bacteria (Korom, 1992; Chowdary et al., 2004; Clement et al., 2002; Senzia et al., 2002). Field studies associated with on-site wastewater nitrogen impacts (DeSimone and Howes, 1998; Rivett et al., 2008) suggest that the availability of sufficient, readily mineralizable carbon, which can be used as an energy source by microbes, is the most critical limitation to denitrification in groundwater.

In this model, we assumed that there is no sorption/desorption of NO_3^--N to/from the subsurface solids, and we used a first-order decay to simulate the process of denitrification; thus,

$$\sum R_n = \lambda\theta C \quad (2)$$

where λ is the first-order decay rate for the dissolved NO_3^--N with unit T^{-1}. Selecting an appropriate decay rate, λ, is always a challenge in modeling. Poeter et al. (2005) noted that the first-order denitrification rates vary widely in literature sources. In this model, a value of 0.006 per day was fit during calibration, which is at the low end of the range reported in the literature (0.004 to 2.27 per day, McCray et al., 2005). This lower value is also consistent with the low organic content detected in the aquifer in the study area.

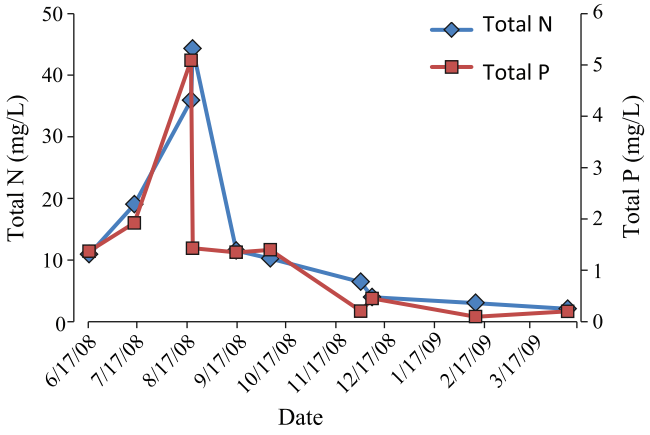

Figure 6. Total nitrogen and phosphorous concentrations of effluent in grab samples taken directly from discharge pipes in the RIBS.

The sorption of P in soils is well documented and is often thought to be associated with metal-oxide minerals that can possess a positive surface charge at typical pH ranges, allowing sorption of the anionic phosphate (Pitt et al., 1996; Stollenwerk, 2003). Sorbed P can then be converted to much less soluble mineraloids or minerals (White and Dornbush, 1988; Pitt et al., 1996). This conversion to low solubility forms has led to models for RIBS design that allow for an infinite attenuation capacity (e.g., Enfield et al., 1981) and are presented in U.S. Environmental Protection Agency (USEPA) guidance documents (USEPA, 2006) and engineering design texts (e.g., Crites et al., 2006). Overloading of P may be especially problematic under RIBS where there has been decades of loading with high concentrations of P and organic carbon (Walter et al., 1995; Stollenwerk, 2003). Detailed field and laboratory experiments have found that as P-rich effluent passes through materials where sorption sites are occupied by phosphate or carbon, the sorption of P from the effluent is low. Further, sorbed P can be released into solution when the concentration of P in groundwater decreases and/or groundwater pH rises to favor desorption (Parkhurst et al., 2003; Stollenwerk 2003).

For the quartzose, sandy soils of the Atlantic Coastal Plain, Pautler and Sims (2000), Maguire and Sims (2002), and Sims et al. (2002) tested the use of a P-sorption ratio (PSR) computed from the Mehlich 3 extractable mole fraction of P divided by the sum of the Mehlich 3 extractable mole fractions of iron (Fe) and aluminum (Al), as an alternative to the more costly and time consuming Langmuir P-sorption isotherm (Nair et al., 1984) and P-sorption index (Mozaffari and Sims, 1994) tests. They found that P-sorption capacities in batch sorption experiments decrease and concentrations of P in leachate from column studies increase once PSR values exceed 0.2. Lower PSR corresponds to higher phosphorous sorption capacity (PSC) as described by James et al. (2005) and Bond et al. (2006). PSR was evaluated on samples from the vadose zone beneath the infiltration basins in this study and in two samples from the saturated zone at Ni45-35, a site just downflow from the RIBS.

Effluent infiltration characteristics within the RIBS also affect P transport during infiltration. In this study, field

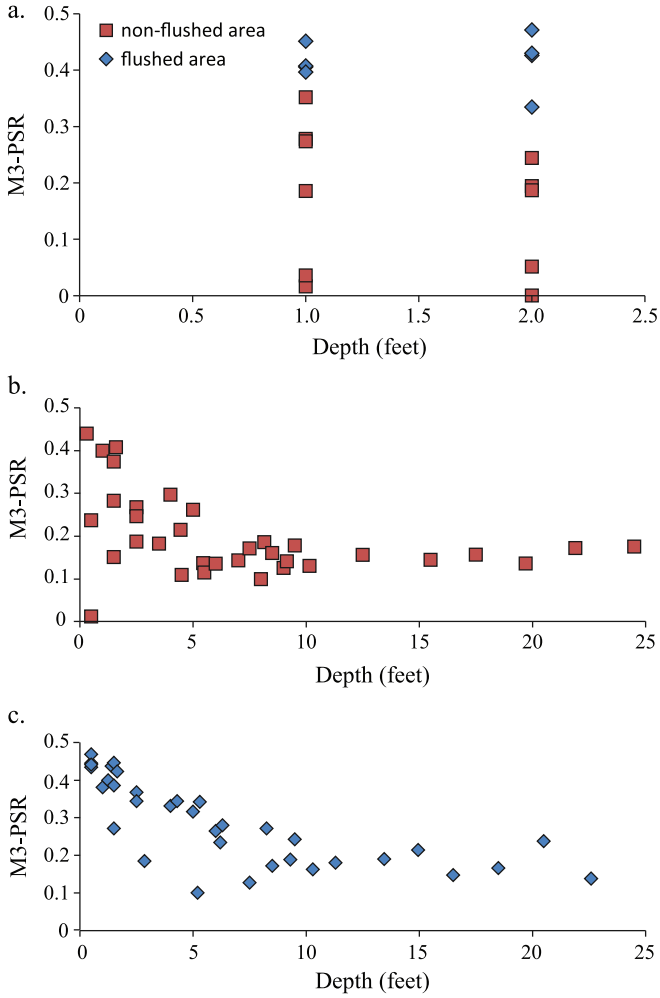

Figure 7. Degree of phosphorous saturation calculated using M3-PSR method. (a) Samples collected from shallow hand auger boreholes (0.6 m), (b) and (c) samples collected from deeper boreholes (7.5 m). Blue diamonds represent the samples collected in frequently flushed areas near discharge pipes, red squares represent the samples collected in non-flushed area located farther from discharge pipes.

observations found nearly all effluent collects and infiltrates within 3 to 5 meters of discharge pipes, leading to significant vegetation growth and soil development within these areas. A majority of soil samples collected at shallow depths (< 60 cm) from sites located near the discharge pipes show PSR values in excess of 0.3 (flushing areas in Fig. 7a) indicating low sorption capacity. A majority of samples collected at shallow depths from sites located farther from discharge pipes (non-flushing areas in Fig. 7a) have much lower PSR values (also lower organic carbon), indicating higher sorption capacity (Fig. 7a). This indicates that PSC of shallow soils (< 0.6 m) has been significantly reduced in areas that receive frequent applications of wastewater.

M3-PSR decreases with depth (Figs. 7b and 7c), and mean M3-PSRs aggregated by depth ranges of 0-0.6, 0.6 to 3, and 3 to 8 m are significantly different (alpha = 0.05). Samples collected close to the discharge pipes (Fig. 7c) have higher M3-PSR values than samples collected farther from the discharge pipes, and M3-PSR exceeds the 0.2 value thought to indicate increased leaching. Though areas that

Table 3. Calibrated parameter values. L1=Layer1, L2=Layer2 and L3=Layer3.

Parameter	Value
Hydraulic conductivity (m/day)	30(L1), 21(L2),15(L3)
Porosity	0.35
Soil bulk density (kg/m^3)	2100
Dispersivity (m)	4
Distribution coefficient for OP (1/(mg/L))	2.7×10^{-6} (outer zone) 4×10^{-7} (inner zone)
First-order decay rate for NO_3^--N (1/day)	0 ~ 0.006

receive frequent applications of wastewater (Fig. 7c) have significantly higher mean M3-PSR (alpha = 0.05) than areas that do not receive frequent applications of wastewater (Fig. 7b) at all depth ranges, the magnitude of the difference between mean M3-PSRs decreases from 0.13 (0 and 0.6 m) to 0.08 (0.6 to 3 m), to 0.02 (3-8 m), thus providing an indication of lateral flow (spreading) and P transport during infiltration through the vadose zone. M3-PSR values in samples collected at Ni45-35 were relatively low ranging from 0.05 (10.3m below land surface) to 0.04 (19.8m below land surface).

Because our work did not include a sophisticated geochemical characterization of sediments (e.g., Stollenwerk, 2003; Parkhurst et al., 2003), we used a combination of the M3-PSR concepts described above and a spatially variable linear sorption isotherm. The linear isotherm model assumes that materials have unlimited sorption capability to simulate sorption/desorption reactions; thus,

$$\sum R_n = -\rho_b \frac{\partial \overline{C}}{\partial t} \text{ and} \quad (3)$$

$$\overline{C} = K_d C \quad (4)$$

Where:

ρ_b Bulk density of the subsurface medium, ML^{-3};

$\overline{C}$ Concentration of phosphorus sorbed on the subsurface solids, MM^{-1};

K_d Distribution coefficient, L^3 M^{-1}.

As mentioned previously, when PSR reaches 0.2, the PSC of soil decreases and leaching of OP increases. To represent the observed reduction of PSC with a linear sorption model, we adopted a double-ring biogeochemical reaction zone by assigning different K_d values in our study domain: an inner ring zone centered on the infiltration basins, with a distribution coefficient (lower PSC) $K_d = 4\times10^{-7}$ (L/mg), and an outer ring with $K_d = 2.7\times10^{-6}$ (L/mg). K_d for the inner ring was obtained through transport calibration of field measured OP; K_d used for the outer ring is that reported by McCray et al. (2005) as a median value for sand material.

RESULTS AND DISCUSSION

Calibration Results

The model-simulated discharge schedule differs from the on-site discharge schedule, as described in the previous section. We used a continuous discharge of wastewater at two hypothesized zones instead of a discontinuous recharge at eight flushing basins (Fig. 3). This simplification does not allow us to fit the simulated head value and contaminant concentrations to the field measurements made under the RIBS in well Ni45-43. However, the errors caused by the simplification are thought to be reduced as the distance between observation points and the RIBS increases. Monthly average water levels and NO_3^--N and OP data from four monitoring wells, Ni45-35, Ni45-36, Ni45-45, and Ni45-37 (Fig. 3), with distances of 40 m, 64 m, 65 m, and 133 m from the center of the RIBS, respectively, were selected for groundwater flow and contaminant transport calibration. Concentrations collected from multi-level wells, CMT3 and CMT2, which are next to standard wells Ni45-35 and Ni45-45, respectively, were also compared with simulation results.

Hydraulic conductivities and recharge rates were adjusted (Table 3) to match the field measurements of water levels (Fig. 8). The first-order decay rate of NO_3^--N (λ) and the distribution coefficient (K_d) of OP (Table 3) were adjusted to match groundwater sampling test results (Figs. 9, 10, 11). Figure 9 shows the simulated break-through curves compared with observations from standard wells Ni45-36 and Ni45-37. No CMT wells were installed with these two standard wells and the calibrated model fits NO_3^--N and OP concentrations quite closely for both wells, as expected. Although the highest concentrations of both NO_3^--N and OP were collected in effluent in August (Fig. 6), the maximum concentration of NO_3^--N was detected in late September (in well Ni45-35; Fig. 10a), while the maximum value of OP was detected in early November (Fig. 10b). As previously discussed, the delay is thought to have been caused by the sorption of a portion of the OP on the aquifer matrix. A slower rate of mineralization of total P to OP compared to organic N and ammonium-N to NO_3^--N in the vadose zone may also have contributed to the delay.

Figure 10 shows the comparison of observed and simulated concentrations NO_3^--N and OP at well Ni45-35 and its paired CMT well (CMT3). This site is located approximately 20 m down flow from the infiltration basins.Although the CMT well and standard well are only 50 cm apart, the concentrations are significantly different, which is thought to be

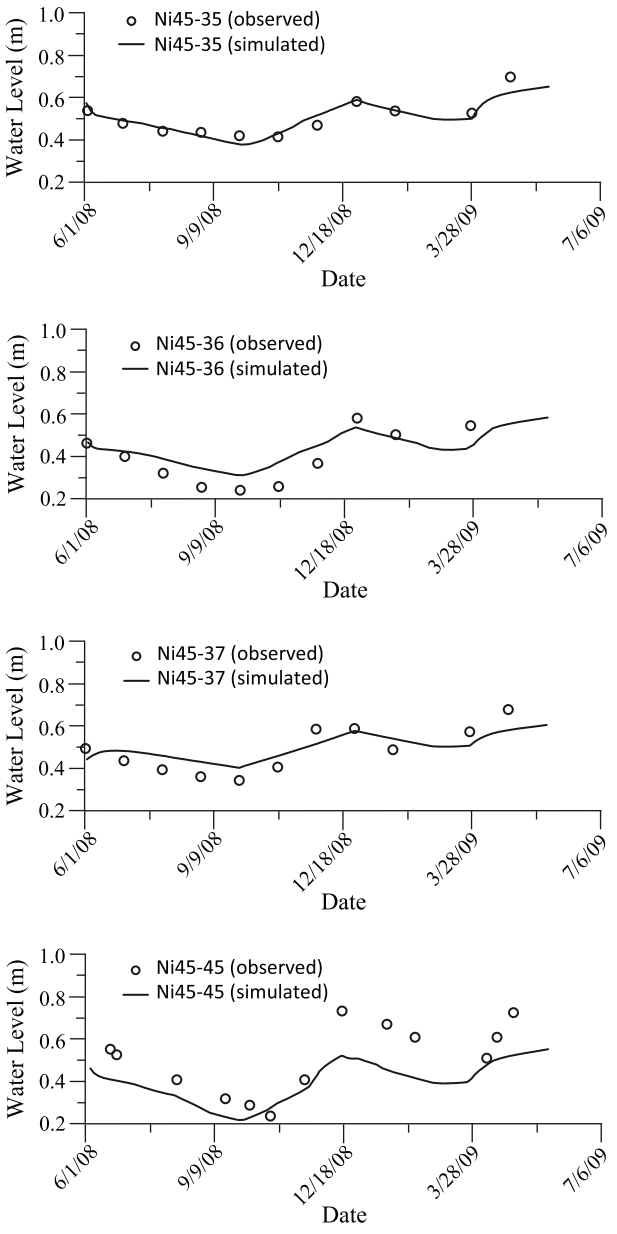

Figure 8. Comparison of observed (circles) and simulated (lines) water-table elevations for monitoring wells Ni45-35, Ni45-36, Ni45-37, and Ni45-45.

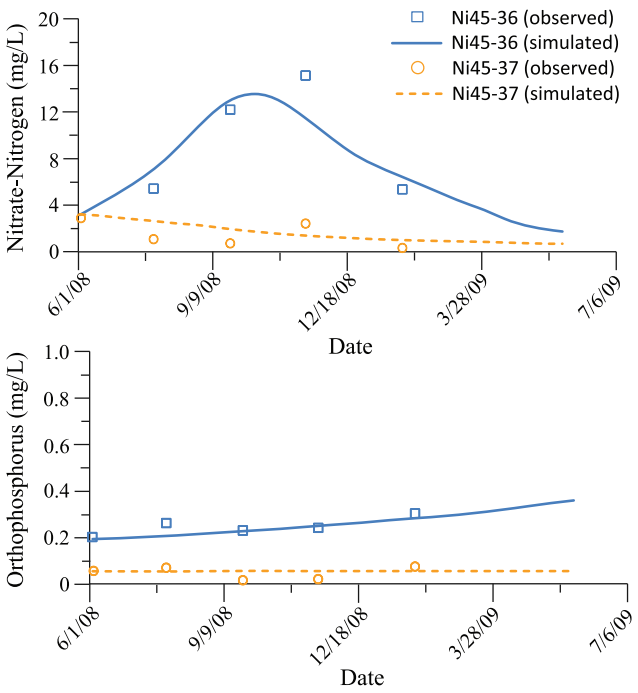

Figure 9. Comparison of observed (symbols) and simulated (lines) NO_3^--N and OP for monitoring wells Ni45-36 and Ni45-37.

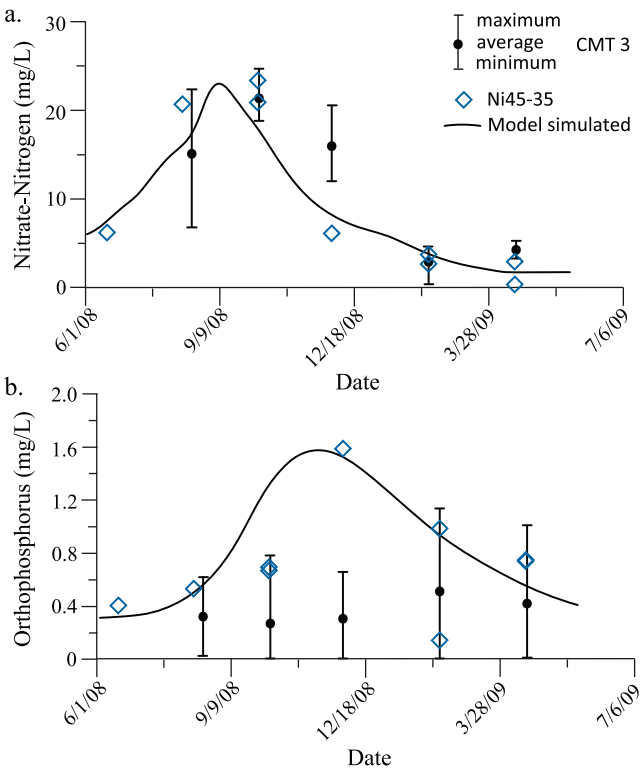

Figure 10. Comparison of observed and simulated NO_3^--N (a) and OP (b) concentrations at well Ni45-35 and CMT3.Diamond symbols show concentrations observed in samples collected from the standard well.On days where two diamonds appear, samples were collected from the top and bottom of the well; otherwise, the sample was collected from the top of the well.Stick and round symbols show concentrations observed in samples collected from CMT3

due to a variety of factors including the different volumes of aquifer contributing to each sample, and the different depths at which the samples were taken.The good fit between the simulated and observed maximum concentrations of NO_3^--N (Fig. 10a) is likely due to: 1) the relatively short distance of the samples from the infiltration basin, and 2) a lack of significant variability in physical and geochemical properties of the aquifer between the infiltration basins and the well site. The simulated OP breakthrough curve can only fit the concentrations collected from the standard well, but is much greater than the averaged concentrations of OP samples collected from CMT3 (Fig. 10b). Although we cannot determine the reason from available data, the heterogeneity of the geochemical properties of the aquifer, the unsampled variability in the contaminant source strength, and the non-representative temporal discretization of contaminant input all likely play important roles.

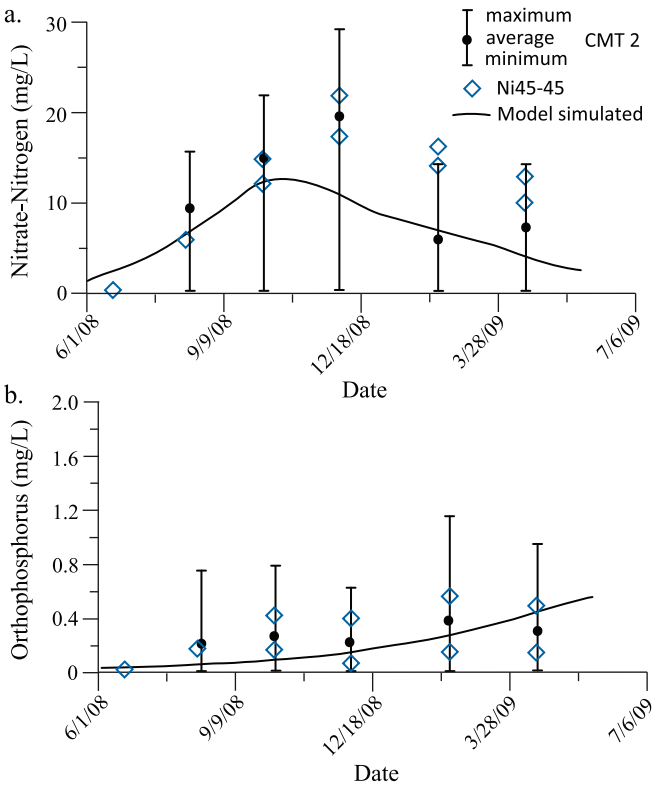

Figure 11. Comparison of observed and simulated NO_3^--N (a) and OP (b) concentrations at well Ni45-45 and CMT2. Diamond symbols show concentrations observed in samples collected from the standard well. On days where two diamonds appear, samples were collected from the top and bottom of the well; otherwise, the sample was collected from the top of the well. Stick and round symbols show concentrations observed in samples collected from the CMT2.

Figure 11 compares observed and simulated concentrations at well Ni45-45 and CMT2. This site is located approximately 65 m down flow of the infiltration basins. The simulated concentrations of NO_3^--N fall in the range of minimum-maximum concentrations collected from CMT2 and the standard well Ni45-45, but underestimate the NO_3^--N peak values that were sampled on 12/2/2008 from the two wells (Fig. 11a). This significant underestimation of NO3--N concentration is thought to be a function of variability in the contaminant source strength, non-representative temporal discretization of contaminant input, rapid groundwater flow rates that transport NO_3^--N faster than can be removed by denitrification, and/or spatially variable physical and geochemical properties in the aquifer. Higher frequency sampling and inclusion of analyses to detect denitrification byproducts are needed to determine the causes of the underestimation. For OP (Fig. 11b), the average concentrations collected from CMT ports and the model-simulated concentrations are nearly bracketed by the range of data from standard wells. It is worth noting that OP concentrations observed in the standard well are lower than the maximum concentrations observed in the CMT well. Simulated concentrations usually under predict the average CMT concentrations and here are a factor of 3 to 7 times smaller than the maximum concentrations in the CMT samples. These findings indicate that geologic and geochemical heterogeneity in the aquifer facilitate preferential transport of NO_3^--N and OP from the site at rates and concentrations much higher than average rates of transport predicted by simulation or detected by standard monitoring wells.

Table 4. Parameters used in Hantush analytical method to calculate mounding height.

Parameter	L (m)	a (m)	K (m/day)	n	t (days)	h_i (m)
Value	56	18	21	0.001	3650	14

K - average for three numerical model layers
n - approximates steady state at 10 years
t - 10 years to approximate steady state

Mounding Analysis

Two different methods used to calculate the maximum mounding beneath the RIBS were compared, the Hantush (1967) analytical model and a modified version of the numerical model discussed previously. Mound heights were calculated by comparing water levels with effluent discharge to water levels with no effluent discharge.

Hantush (1967) introduced an analytical model to determine the rise and fall of the water table in response to uniform recharge under rectangular areas:

$$h_m = \sqrt{h_i^2 + \left(\frac{2w}{K}\right) vt S^*\left(\frac{l}{\sqrt{4vt}}, \frac{a}{\sqrt{4vt}}\right)} \quad (5)$$

$$S^*(\alpha, \beta) = \int_0^1 erf\left(\frac{\alpha}{\sqrt{\tau}}\right) \cdot erf\left(\frac{\beta}{\sqrt{\tau}}\right) d\tau \quad (6)$$

Where:

h_m	maximum height of the water table
h_i	initial height of the water table
K	hydraulic conductivity
w	discharge rate
t	time since discharge begins
v	Kb/n
n	specific yield
l	one - half length of area of recharge
a	one - half width of area of recharge
b	$(h_i+h(t))/2$

In this case, the parameters used in the Hantush analytical method are the same as those used in the numerical model (Table 4).

In order to estimate how the maximum mound height may change due to variations in discharge, five different discharge rates equivalent to those used in the numerical model were used in the Hantush (1967) model.

A comparison of results illustrates good agreement between these two methods (Fig. 12). This is thought to be partially due to the relatively spatially uniform hydraulic properties in the study area, which meet the assumption of a homogeneous aquifer, as used in the Hantush method. The

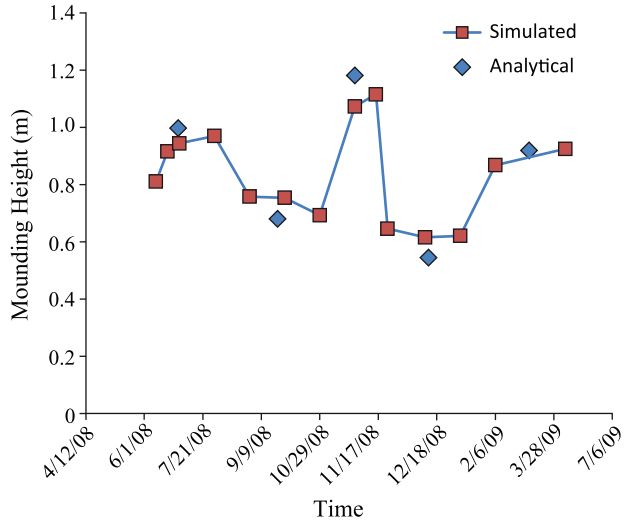

Figure 12. Comparison of maximum groundwater mounding beneath RIBS computed by analytical and numerical modeling methods (simulated).

Hantush method overestimates the mounding height using maximum discharge rates and underestimates the mounding height with minimum discharge rates when compared to the numerical simulation. This is expected because the Hantush method assumes that a steady-state flow condition was achieved in the system, a condition that was not reached in the field.

Mass Balance Analysis of N and P

Based on mass balance analysis, a total of 759 kg of N were added into the aquifer through the RIBS during the modeling period. During the simulation, the total mass of N in the aquifer decreased from 3496 kg in June 2008 to 2578 kg in June 2009 due to denitrification and discharge through the model boundaries. Approximately 73 percent of the reduction of the total mass of N was caused by denitrification.

Based on a mass balance analysis, a total of 83.86 kg P were added into the aquifer through the RIBS during the modeling period. Because the only mechanism of P transformation considered in the model was linear sorption/desorption, the mass of P can only leave the model domain through flow boundaries. During the simulation, approximately 3.66 kg of P were discharged through boundaries and 80.2 kg of P were accumulated in the aquifer. A comparison of the amount of P in the aquifer at the end of the simulation (383.74 kg), with the sum of the initial amount of P in the aquifer plus the amounts added and lost during the simulation, indicates that more than 99 percent of P was retained in the model area. Obviously, the long-term accumulation of P will reduce the sorption capacity of the RIBS porous medium. Multi-year simulations could provide information for assessing the timing of P breakthrough.

Sensitivity Analysis

Sensitivity analysis is used to determine the sensitivity of a model to changes in the values of its parameters. In this study, a set of the input parameters (hydraulic conductivity, decay rate of NO_3^--N, sorption coefficient of OP, dispersion, recharge rate of effluent, and recharge contaminants concentrations) was chosen to calculate the relative sensitivities using the following equation:

$$S_\alpha^F = \frac{\%\text{change in } F}{\%\text{change in } \alpha} = \frac{\Delta F/F}{\Delta\alpha/\alpha} \quad (7)$$

where S_α^F is the relative sensitivity of the model output parameter F with respect to the model input parameter α.

By increasing one parameter by 50 percent, while keeping the other parameters unchanged, we compared the total mass (solid phase and liquid phase) changes in the aquifer after a one-year simulation. Because most of the OP is detained in the aquifer, the increments of recharge rate and recharge concentration lead almost to the same amount of OP in the aquifer (Fig. 13), while the other parameters play a negligible role in changing the total mass in the aquifer. Compared to the sorption coefficient of OP, the decay rate (denitrification rate) of NO_3^--N plays a more important role in reducing the total mass in the aquifer. These results indicate that the best means of reducing the total mass detained in the aquifer is to reduce the recharge rate or the recharge concentration of the contaminants. To reduce NO_3^--N concentrations, increasing denitrification capability by improving redox conditions may be an effective alternative.

Comparison of 2-D and 3-D Particle Pathlines

As a first approximation of the flow of effluent away from the infiltration basins, Andres et al. (2015) used the two-dimensional (2-D) particle tracking feature of the ArcMap Hydrology toolbox (ESRI, 2008). The initial positions of the particles, representing effluent, were set along the boundaries of the infiltration basins, and average-annual water-table elevations from monitoring wells and estimated elevations of tidal water bodies were used to determine the head distribution in the aquifer. Hydraulic conductivity in the model domain consisted of two zones, determined from slug tests and geological mapping. The greater K-zone was assigned to the generally coarse-grained, dune- and spit-complex deposits. The lower K-zone was assigned to the swamp deposits. The effective porosity was set to 0.25 and thickness was set to 30 ft over the entire domain.

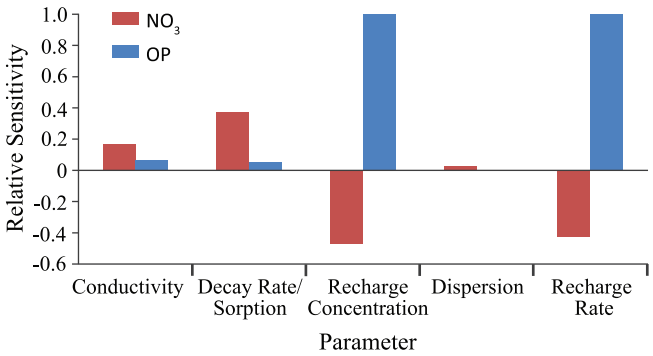

Figure 13. Plot of sensitivity analysis results for the calibrated model testing hydraulic conductivity, decay rate (for NO_3^--N)/sorption coefficient (for OP), recharge concentrations of wastewater, dispersion, and wastewater recharge rate.

The particle pathlines computed by the 2-D steady-state model radiate outward from the infiltration basins in all directions (Fig. 14). The longest pathlines, coincident with the greatest hydraulic gradients, are directed toward the south to the sea-level swamp. Particle velocities range from 0.55 ft/d to 1.8 ft/d with the greatest velocities directed toward the sea-level swamp.

In map view, particle pathline orientations computed from the transient one-year, 3-D simulation (Fig. 15a) are generally similar to those computed by the 2-D model (Fig. 13). Nearly all of the pathlines (38 of 40) from the steady-state, 2-year simulation (Fig. 15b) turn to the south and move along the path of steepest hydraulic gradient towards the sea-level swamp. These pathlines indicate that it is unlikely that a significant mass of contaminants flowed toward previously unmonitored areas located northwest and northeast of the infiltration basins.

Cross-sectional views of 3-D particle pathlines show a significant vertical component of flow (Fig. 16). This component is greatest directly under the infiltration basins and decreases with distance from the basins. The particle pathlines show that effluent first flows downward through the aquifer and then laterally as the water moves away from the infiltration basins. This also explains the apparent slower horizontal transport of effluent from the infiltration basins than that predicted by the 2-D model.

The vertical component of flow also creates complex spatial and temporal distributions of contaminants. The top of the effluent mass occurs farther beneath the water table with increasing distance from the infiltration basins until the effluent mass approaches the sea-level swamp. For example, samples collected from the water table at location A (Fig. 16) would not be representative of the main mass of RIBS effluent in the aquifer. A sample collected from near the bottom of the aquifer at the same time and location, would also not detect the main mass of RIBS effluent, which would reach this location at a later time. This complex vertical variability of concentrations was observed in the CMTs at CHSP.

One interesting feature seen in cross-section is that the pathlines originating at the northern edge of the infiltration basin initially have downward and northward components (Fig. 16). With time, some of the pathlines reverse direction toward the south.

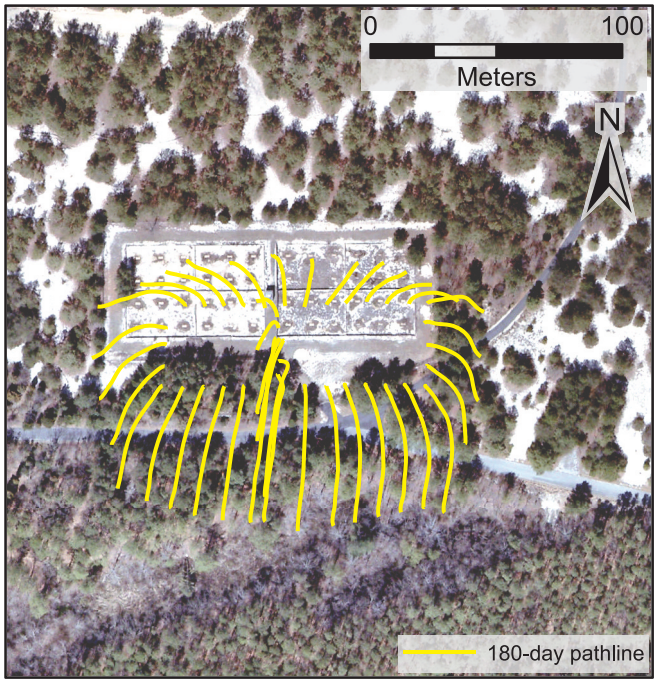

Figure 14. Particle pathlines computed by the 2-D steady-state model. Simulation length is 180 days. Illustration modified from Andres et al. (2010).

a.

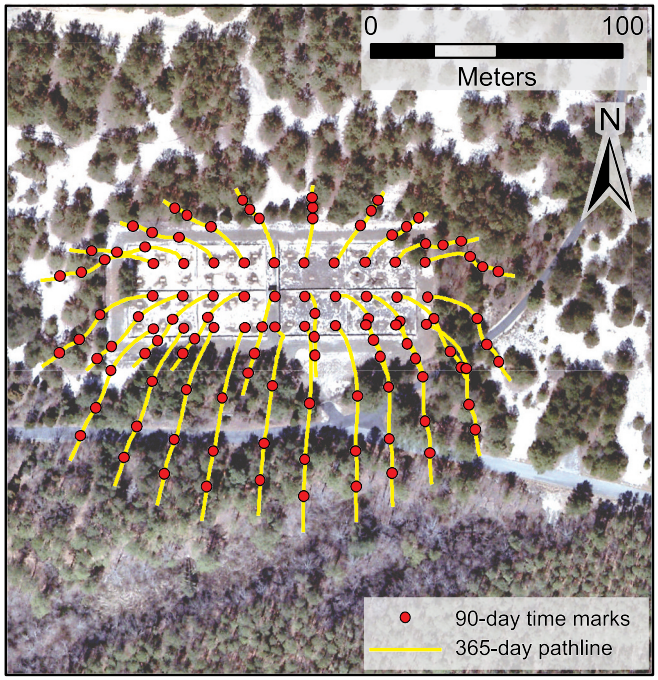

b.

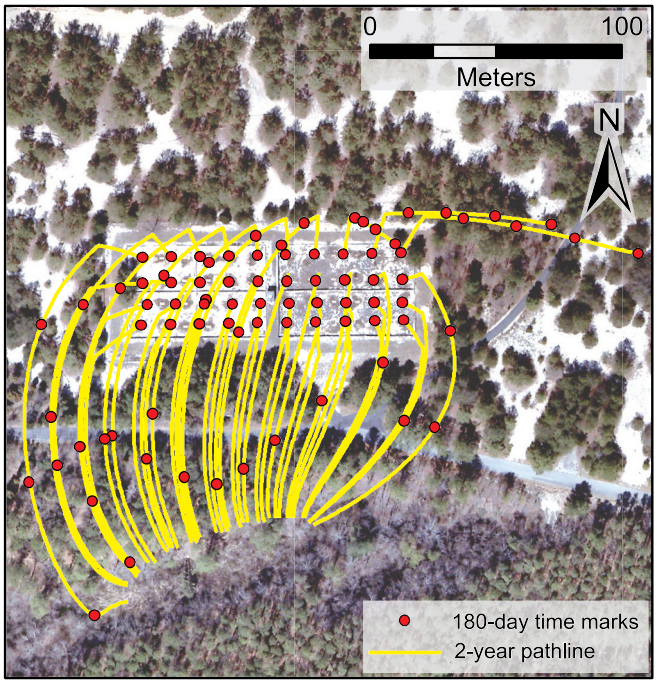

Figure 15. Particle pathlines computed by the 3-D model. (a) 365-day transient simulation. The red dots on the tracking lines are placed at 90 day intervals. (b) 2-year steady-state simulation. The red dots are placed at 180 day intervals.

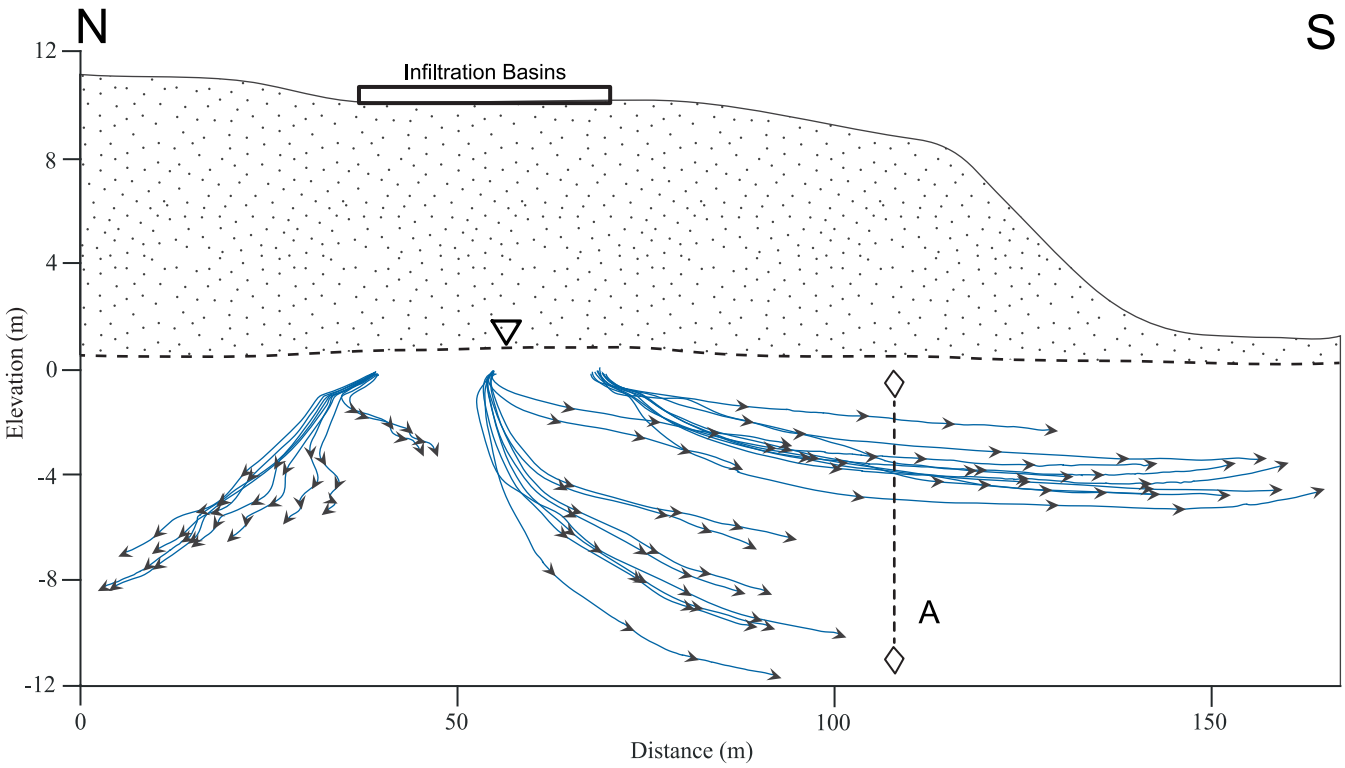

Figure 16. Cross-sectional view of one-year particle pathlines computed by the 3-D model. Tick marks represent 90-day intervals. This view is a north-south oriented column located through the center of the array of infiltration basins. The diamond symbols represent hypothetical sample points that are discussed in the text.

CONCLUSIONS

A variety of field experiments were conducted to evaluate the risks of RIBS on the local groundwater environment at Cape Henlopen State Park in southern Delaware. The major contaminants of concern are NO_3^--N and OP, which were simulated using a 3-D contaminant transport model. The following conclusions were made based on the outcome of this work:

1. The simple, lower-cost analytical Hantush mounding method can simulate a relatively accurate estimate of steady-state groundwater mounding (approximately 10 percent difference compared to numerical modeling) under a relatively homogeneous unit.
2. Simulations using a small denitrification rate, coupled with effluent inputs averaged over quarterly time steps and the entire discharge area, predict that the total mass of NO_3^--N was reduced by 62 percent in the study domain. However, simulations significantly under predict observed NO_3^--N concentrations at downflow multi-port CMT wells, indicating that simulated denitrification rates are too large, and/or preferential flow of NO_3^--N through geological and geochemical heterogeneities are important pathways for NO_3^--N transport. These points raise interesting issues for determining how well SAT can remediate N. Further, it is likely that transport models that do not use detailed discretization of contaminant input are too oversimplified to accurately simulate N-transport and attenuation processes.
3. The long-term operation of RIBS has led to a reduction of the sorption capacity of subsurface solids for phosphorous, resulting in significant concentrations of OP in groundwater. Simulations that use a simple spatially variable linear isotherm to reflect the loss of sorption capacity under the RIBS, coupled with effluent inputs averaged over quarterly time steps and the entire discharge area, predict that most of the OP can be contained in the model domain and predicted OP concentrations appear to partially fit observed average OP concentrations. However, simulations significantly under predict observed OP concentrations in downflow multi-port CMT wells, indicating that the P-sorption model and/or the crude discretization of contaminant input used in the simulation may be too simplified. The preferential flow of OP through geological and geochemical heterogeneities cannot be discounted. These points indicate that transport models based on simple sorption isotherms are not adequate to accurately predict P transport and attenuation processes.
4. Comparisons indicate that concentrations observed in standard wells somewhat reasonably fit simple averages from the multi-port CMT wells. However, these concentrations observed frequently are much smaller than the maximum concentrations observed in CMT wells. This phenomenon is reproduced by 3-D particle track modeling and is illustrative of complex time-variant, 3-D flow paths and contaminant plume shapes. This complexity raises interesting issues for designing systems for compliance monitoring of RIBS/SAT.

5. The particle tracking done in 3-D simulations predict that vertical flow paths are significant near the RIBS. These findings are qualitatively similar to water quality observations in the vertically nested sample points in CMTs. A comparison with results from 2-D simulations indicates that 2-D simulations are inappropriate for use in modeling effluent flow from RIBS. Additional research is now being conducted to determine if loading rates similar to those used in spray irrigation cause significant vertical flow.

REFERENCES CITED

Andres, A.S., 1991, Results of the Coastal Sussex County, Delaware Ground-Water Quality Survey: Delaware Geological Survey Report of Investigation No. 49, 28 p.

Andres, A. S., Walther, E. F., Turkmen, M., and He, C., 2015, Hydrogeology of a rapid infiltration basin system at Cape Henlopen State Park, Delaware: Delaware Geological Survey Bulletin 21B, 43 p.

Asano, T., Burton, F.L., Leverenz, H.L., Tsuchihashi, R., and Tchobanoglous, G., 2007, Water Reuse; Issues, Technologies and Applications: New York, NY, McGraw-Hill, 1570 p.

Ator, S. W., 2008, Natural and Human Influences on Water Quality in a Shallow Regional Unconsolidated Aquifer, Northern Atlantic Coastal Plain: U.S. Geological Survey Scientific Investigations Report 2008-5190, 32 p.

Bond, C. R., Maguire, R. O. and Havlin, J. L., 2006, Change in Soluble Phosphorus in Soils following Fertilization is Dependent on Initial Mehlich-3 Phosphorus: Journal of Environmental Quality, v. 35, p. 1818-1824.

Bouwer, H., 1989, The Bouwer and Rice slug test - an update: Ground Water 27, p. 304-309.

Chowdary, V.M., Rao, N. H. and Sarma, P. B. S., 2004, A coupled soil water and nitrogen balance model for flooded rice fields in India: Agriculture, Ecosystems and Environment v. 103, p. 425–441.

Clement, J. C., Pinay, G., Marmonier, P., 2002, Seasonal dynamics of denitrification along topohydrosequences in three different riparian wetlands: Journal of Environmental Quality v. 31, p. 1025–1037.

Crites, R.W., Middlebrooks, E.J., and Reed, S.C., 2006, Natural Wastewater Treatment Systems: New York, NY, Taylor & Francis Group, 552 p.

Debrewer, L. M., Ator, S. W., and Denver, J. M., 2005, Factors Affecting Spatial and Temporal Variability in Nutrient and Pesticide Concentrations in the Surficial Aquifer on the Delmarva Peninsula: U.S. Geological Survey Scientific Investigations Report 2005-5257.

Denver J. M., Ator, S. W., Debrewer, L.M., Ferrari, M.J., Barbaro, J.R., Hancock, T.C., Brayton, M.J., and Nardi, M.R., 2004, Water Quality in the Delmarva Peninsula, Delaware, Maryland, and Virginia, 1999–2001, U.S. Geological Survey Circular 1228, 30 p.

DeSimone, L. A., and Howes, B. L., 1998, Nitrogen transport and transformations in a shallow aquifer receiving wastewater discharge, a mass balance approach: Water Resources Research v. 34, p. 271-285.

Enfield, C. G., Phan, T., Walters, D. M., 1981, Kinetic model for phosphate transformation in calcareous soils: II. Laboratory and field transport: Soil Science Society of America Journal, v. 45, p. 1064-1071.

ESRI, 2008, ArcInfo v. 9.2: Redlands, CA.

Golden Software, 2008, Surfer v.9: Golden CO.

Guitierrez-Magness, A. L., and Raffensperger, J. P., 2003, Development, Calibration, and Analysis of a Hydrologic and Water-Quality Model of the Delaware Inland Bays Watershed: U.S. Geological Survey Water Resources Investigation Report 03-4124, 46 p.

Hantush, M. S., 1967, Growth and decay of groundwater mounds in response to uniform percolation: Water Resources Research v. 3, p. 227-234.

Heatwole, K., K., and McCray, J., E., 2007, Modeling potential vadose-zone transport of nitrogen from onsite wastewater systems at the development scale: Journal of Contaminant Hydrology v. 91, p. 184–201.

James, W.F., Barko, J.W., and Soballe, D.M., 2005, Phosphorus saturation characteristics in relation to land-use practice for soils in the upper Eau Galle River watershed, Wisconsin: ERDC WQTN-PD-17.

Johnston, R. H., 1976, Relation of ground water to surface water in four small basins of the Delaware Coastal Plain: Delaware Geological Survey Report of Investigations No. 24, 56 p.

Korom, S., F., 1992, Natural denitrification in the saturated zone: A review: Water Resources Research v. 28, p. 1657–1668.

Ling, G., and Ei-Kadi, A. I., 1998, A lumped parameter model for nitrogen transformation in the unsaturated zone: Water Resources Research v. 34, p. 203–212.

Maguire, R. O., and Sims, J. T., 2002, Measuring Agronomic and Environmental Soil Phosphorus Saturation and Predicting Phosphorus Leaching with Mehlich 3: Soil Science Society of America Journal, v. 66, p. 2033-2039.

McCray, J. E., Shiloh, L. K., Siegrist, R. L., and Thyne, G., D., 2005, Model Parameters for Simulating Fate and Transport of On-Site Wastewater Nutrients: Ground Water v. 43, p. 628-639.

Miller, J.C., 1972, Nitrate Contamination of the Water-Table Aquifer in Delaware: Delaware Geological Survey Report of Investigations No. 20, 36 p.

Mozaffari, P.M., and Sims, J.T., 1994, Phosphorus availability and sorption in an Atlantic Coastal Plain watershed dominated by intensive, animal-based agriculture: Soil Science, p. 97–107.

Nair, P.S., Logan, T.J., Sharpley, A.N., Sommers, I.E., Tabatabai, M.A. and Yuan, T.L., 1984, Interlaboratory comparison of a standardized phosphorus adsorption procedure: Journal of Environmental Quality, p. 591–595.

Parkhurst, D. L., Stollenwerk, K. G., and Colman, J. A., 2003, Reactive-transport simulation of phosphorus in the sewage plume at Massachusetts Military Reservation, Cape Cod, Massachusetts: US Geological Survey Water-Resources Investigation Report -03-4017, 33 p.

Pautler, M. C., and Sims, J. T., 2000, Relationships between soil test phosphorus, and phosphorus saturation in Delaware soils: Soil Science Society of America Journal, v. 64: p. 765-773.

Pellerito, V., Neimester, M.P., Wolff, E., and Andres, A.S., 2006, Results of the Domestic Well Water Quality Study: Delaware Geological Survey Open File Report No. 48, 50 p.

Pitt, R., Clark, S., Parmer, K., and Field, R., 1996, Groundwater contamination from stormwater infiltration: CRC Press .

Poeter, E., McCray, J., Thyne, J. and Siegrest, R., 2005, Guidance for evaluation of potential groundwater mounding associated with cluster and high-density wastewater soil absorption systems: International Groundwater Modeling Center, Colorado School of Mines, Golden, CO, NDWRCDP Project Number WU-HT 02-45.

Ritter, W.F., and Chirnside, A.E.M., 1984, Impact of Land Use on Ground-Water Quality in Southern Delaware: Ground Water, v. 22, p. 38-47.

Rivett, M. O., Buss, S. R., Morgan, P., Smith, J. W. N., and Bemment, C. D., 2008, Nitrate attenuation in groundwater: A review of biogeochemical controlling processes: Water Research v. 42, p. 4215-4232.

Robertson, F.W., 1977, The quality and potential problems of ground water in coastal Sussex County, Delaware: University of Delaware Water Resources Center, 58 p.

Senzia, M. A., Mayo, A. W., Nbwette, T.S.A., Katima, J.H.Y., Jorgensen, S.E, 2002, Modeling nitrogen transformation and removal in primary facultative ponds: Ecologic Modeling v. 154, p. 207–215.

Sims, J. T., Andres A. S., Denver, J.M., and Gangloff, W.J., 1996, Assessing the impact of agricultural drainage on ground and surface waters in Delaware: University of Delaware Department of Plant and Soil Science.

Sims, J. T., Maguire, R. O., Leytem, A. B., Gartley, K. L., and Pautler, M. C., 2002, Evaluation of Mehlich 3 as an agri-environmental soil phosphorus test for the Mid-Atlantic United States of America: Soil Science Society of America Journal, v. 66, p. 2016-2032.

Stollenwerk, K. G., 2003, Simulation of phosphate transport in sewage-contaminated groundwater, Cape Cod, Massachusetts: Applied Geochemistry, v. 11, p. 317-324.

Ullman, W. J., Andres, A. S., Scudlark, J. R., and Savidge, K. B., 2002, Storm-water and baseflow sampling and analysis in the Delaware Inland Bays: preliminary report of findings 1998-2002: Open-File Report No. 44, Delaware Geological Survey, 40 p.

US Environmental Protection Agency, 2006, Process Design Manual Land Treatment of Municipal Wastewater Effluents: U.S. Environmental Protection Agency Report EPA/625/R-06/016.

Walter, D. A., Rea, B. A., Stollenwerk, K. G., and Savoie, J., 1995, Geochemical and hydrologic controls on phosphorus transport in a sewage-contaminated sand and gravel aquifer near Ashumet Pond, Cape Cod, Massachusetts: US Geological Survey Water Supply Paper 2463.

White, E. M., Dornbush J. M., 1988, Soil change caused by municipal waste water applications in eastern South Dakota: Water Resources Bulletin v. 24, p. 269-273.

Zheng, C., and Wang, P.P., 1999, MT3DMS: a modular three-dimensional multispecies transport model for simulation of advection, dispersion, and chemical reactions of contaminants in groundwater systems; documentation and user's guide: Contract Report SERDP-99-1, U.S. Army Engineer Research and Development Center, Vicksburg, MS.

Delaware Geological Survey
University of Delaware
Newark, Delaware 19716